

Toward real-time rigid registration of intra-operative ultrasound with preoperative CT images for lumbar spinal fusion surgery

Housseem-Eddine Gueziri · Simon Drouin · Charles X.
B. Yan · D. Louis Collins

Received: date / Accepted: date

Abstract

Purpose Accurate and effective registration of the vertebrae is crucial for spine surgical navigation procedures. Patient movement, surgical instrumentation or inadvertent contact with the tracked reference during the intervention may invalidate the registration, requiring a rapid correction of the misalignment. In this paper, we present a framework to rigidly align pre-operative computed tomography (CT) with the intra-operative ultrasound (iUS) images of a single vertebra.

Methods We use a single caudo-cranial axial sweep procedure to acquire iUS images, from which the scan trajectory is exploited to initialize the registration transform. To refine the transform, locations of the posterior vertebra surface are first extracted, then used to compute the CT-to-iUS image intensity gradient-based alignment. The approach was validated on a lumbosacral section of a porcine cadaver.

Results We achieved an overall median accuracy of 1.48 mm (success rate of 84.42%) in ~ 11 s of computation time, satisfying the clinically accepted accuracy threshold of 2 mm.

Conclusion Our approach using intra-operative ultrasound to register patient vertebral anatomy to pre-operative images matches the clinical needs in terms of accuracy and computation time, facilitating its integration into the surgical workflow.

Keywords Spine surgery · Registration · Ultrasound · Computed tomography · Vertebra · GPU acceleration

1 Introduction

Over 400,000 spinal fusion procedures are performed annually in the United States [1], with a 56.4% increase between 2003 and 2012 [2]. Spinal fusion surgery is the standard of care procedure for treating various spinal conditions involving scoliosis, spinal stenosis, degenerative disc disease and spondylolisthesis [1]. During surgery, pedicle screws are used to fix metal plates and rods to support the spine. However, the procedure is challenging and associated with potentially high neurological, vascular or mechanical complication risks [3–5]. Image-guided surgery (IGS) systems demonstrated a significant decrease in breach and screw malpositioning rates [6–8] by providing spatial positions of tracked surgical instruments in the operative field. During navigation, a rigid registration procedure is performed to align the patient’s anatomy to pre-operative images. In addition, a dynamic reference object (DRO) is rigidly attached to a vertebra and serves as a reference coordinate frame to account for patient position and motion during surgery.

In a standard clinical procedure, registration is achieved with landmark-based technique, by manually identifying homologous anatomical landmarks on both the images and the patient. The procedure can take

H.-E. Gueziri, S. Drouin, C. X. B. Yan and D. L. Collins
McConnell Brain Imaging Center, Montreal Neurological Institute and Hospital, WB221, 3801 University Street, Montreal, QC H3A 2B4, Canada
E-mail: houssem.gueziri@mcgill.ca, louis.collins@mcgill.ca

C. X. B. Yan
Department of Medical Imaging, University of Toronto, 263 McCaul Street, Toronto, ON M5T 1W7, Canada

10 to 15 minutes for each vertebra [9,10]. This approach is tedious, extends the operating time and is subject to operator variability. Commercial navigation systems for spine surgery, e.g., the O-arm (Medtronic inc., Minneapolis, MN), enable acquisition of 2D fluoroscopy or 3D computed tomography (CT) intra-operative images. This provides updates of the anatomy and instrument locations during surgery [5,8,11], but introduces risks of harmful radiation exposure for both the patient and the operating room (OR) personnel [12,13]. Moreover, the setup time is ~ 15 minutes [14] and extra personnel is required for equipment manipulation, which further extends the surgical procedure time and costs.

Another important issue in spine IGS is the loss of accuracy as the surgery duration increases [15]. Patient movement, surgical actions such as drilling or tapping, and inadvertent contact with the DRO may invalidate the registration. While intra-operative ultrasound (iUS) provides the ability to acquire images that can be used to correct for misregistration during surgery, the overall procedure is time demanding in the surgical workflow. Current iUS-based registration techniques require 2 to 5 minutes per vertebra [16–19], precluding frequent registration corrections. In addition, a manual landmark-based registration is commonly performed to initialize the registration transform. Our goal is to achieve frequent and accurate re-registration with minimal or no impact on the overall surgery time. In a preliminary work [20], we presented a framework for a fast *rigid* CT-to-iUS image registration of a *single vertebra*, designed for spinal fusion surgery. This paper provides further analysis and validation to explore the effects of iUS acquisition variability on the registration accuracy.

2 Related work

2.1 CT-to-iUS registration

A common approach to register CT to iUS images for spine surgery is to use the posterior surface of the vertebra. Yan et al. [9,16] proposed to maximize the intensity cross-correlation of the posterior vertebra surface. The reported median target registration error (TRE) ranged between 1.65-2.31 mm on porcine cadavers. A slice-to-volume variant of the approach proposed in [17], in which the registration is performed without iUS volume reconstruction to accelerate the computations, achieved comparable accuracy with registration time around 120 s per vertebra. Koo et al. [18] extended the approach by including an additional intensity-based rigid registration step performed between the vertebra surface on the CT image and the original iUS image. The average TRE reported was $2.18 \text{ mm} \pm 0.82 \text{ mm}$ (ranging between 0.89-4.45 mm) on a porcine cadaver. The registration was achieved in ~ 100 s per vertebra.

In order to avoid errors related to iUS surface extraction, Brendel et al. [21] proposed to use a surface-to-volume registration, by maximizing the sum of the iUS gray levels at the CT vertebral surface locations. The approach was used to successfully register the lumbar segment of an ex vivo human spine preparation. Winter et al. [22] used a similar approach with additional pre-processing of iUS images to enhance the bone surface. The accuracy was reported in terms of points-to-surface distances and showed good results under small initial misalignments (below 10 mm translation and 12° rotation), achieving the best success rate of 88.4% under 1 mm distance.

To account for spine curvature, Gill et al. [23] used a biomechanical model to represent coherent inter-vertebral structure displacement between independently registered vertebrae. Alignment of each vertebra is obtained by performing an intensity-based rigid registration of an ultrasound-simulated image calculated from the CT image with the real iUS image. The reported average TRE ranged from 0.62 mm to 2.26 mm for an average computation time of 43 min. In order to reduce the computation time, the same group [24] proposed a spring-based biomechanical model to account for inter-vertebral disc motion. The model acts as an inter-vertebral spring force used as a regularization term in a point-based registration [25]. The average accuracy was 2.2 mm on lumbar segment of a sheep cadaver for 15 min of computation time.

Nagpal et al. [19] proposed a multi-vertebrae CT-to-iUS registration framework. First, a point-based registration is achieved using the vertebra surface points extracted from iUS and CT images. To account for the spine curvature over multiple vertebrae, an additional group-wise vertebra registration is performed, in which intervertebral points are manually added to prevent physically incoherent transformations. Because the study was conducted on clinical data of human subjects, a ground truth registration was not available. The authors used manual landmark registration combined with the proposed method to serve as ground truth registration. They reported average TRE of anatomical landmarks ranging from 0.71-1.70 mm and

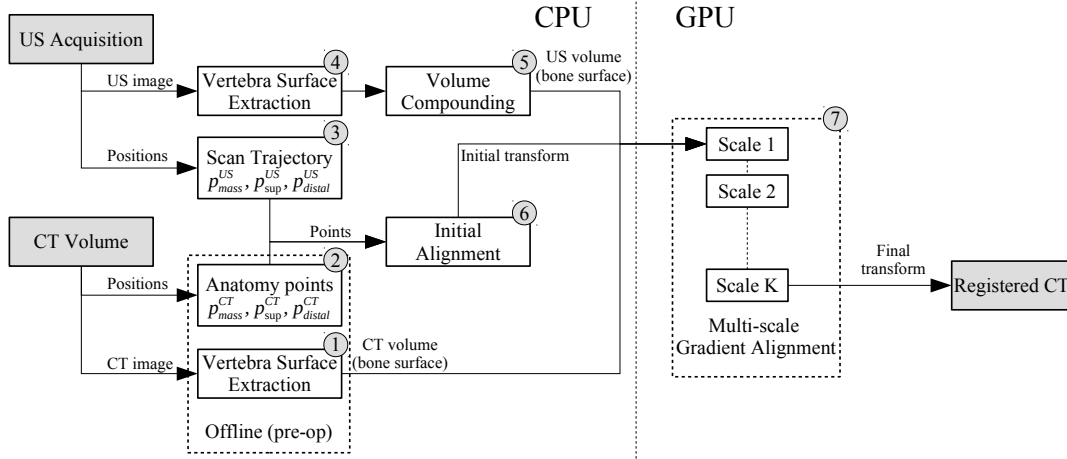


Fig. 1: Flowchart of the proposed registration framework.

a computation time ranging from 50-185 s, excluding the time required by the operator to manually set intervertebral points.

2.2 Clinical limitations

A common limitation of the aforementioned approaches is the need of an initial alignment, required under the assumption of a small initial misalignment. This is expected to be achieved prior to the registration with a landmark-based manual registration. Although Nagpal et al. [19] prevented this step by assuming the same anatomical structures (i.e., the same number of vertebrae) to be imaged in both iUS and CT scans, the initial alignment is obtained by applying an intensity-based registration, which may be computationally expensive. Another clinical issue often neglected is the variability and the duration of the iUS acquisition procedure during surgery. As the acquisition is performed intra-operatively, pre-processing, such as volume reconstruction and vertebra surface extraction, needs to be performed shortly after the acquisition. However, the computation time of the pre-processing tasks has not been reported in the aforementioned works. While an accurate bone extraction method takes approximately 9 s per image [26], a straightforward ray tracing approach would be less accurate but much faster. In this paper, a compromise between accuracy and computation time is considered while designing our registration approach.

3 Image registration

An overview of our registration framework is shown in Fig. 1. The pre-operative stage involves two steps: extract the posterior surface of the vertebra in CT images (1), and extract CT anatomy orientation points (2). During the surgery, five intra-operative steps are performed: extract probe’s trajectory points (3), extract the posterior surface of the vertebra in iUS images (4), create an iUS compounded volume from iUS acquisition slices (5), estimate the initial alignment using the iUS scan trajectory and the CT anatomy points (6), and perform a multi-scale gradient alignment of the vertebra surfaces of CT and iUS images (7). Note that the posterior vertebra surfaces on CT were extracted using the forward tracing method [9]. A similar approach was used on 2D iUS images. However, surface points on iUS correspond to the position where the maximum value was encountered on the tracing. In addition, because we use gradient information in the final alignment step, the resolution of the iUS compounded volume is to be taken into account as a too sparse volume precludes capturing inter-slice gradient information. This will be discussed in the experimental validation.

3.1 Intra-operative ultrasound image acquisition

Ultrasound images were acquired using a locally developed IGS system composed of an optical tracking camera (Polaris, Northern Digital Inc., ON, Canada), an ultrasound machine with a tracked phased array probe (HDI 5000/P4-7, Philips, Amsterdam, Netherlands) and a tracked tool used as a DRO. A saline solution (0.9% NaCl) is poured into the cavity to facilitate ultrasound propagation. Isotonic saline solutions are commonly used in open surgeries to irrigate, rinse or improve image quality. The *Intraoperative Brain Imaging System* (IBIS) [27] open-source platform was used to calibrate the probe, visualize 3D data and record the iUS acquisitions. Similar to an image-guided surgery procedure, the spatial position and orientation of tracked tools and intra-operative images were recorded relative to the DRO coordinate system. In order to reduce computation time, the iUS acquisition was sub-sampled so that a minimum distance $d \in \mathbb{R}_{\geq 0}$ separates the center point of successive frames. A high value of d yields a sparse volume and fast computations, while a value of zero does not modify the acquisition. The frames satisfying the distance criterion are processed in the next steps.

3.2 Ultrasound volume compounding

The ultrasound frames are combined into a single volume by aggregating the ultrasound slices to form a resampled volume, called the compounded volume. This avoids a full volume reconstruction by interpolating in-between slice voxels, as proposed in [17]. Because the relationship between the spatial positions of the ultrasound slices is fixed, registering the compounded volume to the CT volume is analogous to simultaneously optimizing for a slice-to-volume rigid body registration of each individual iUS slice to the CT volume. In our implementation, each iUS pixel intensity is resampled in its corresponding 3D location in the compounded volume, and the intensities are averaged for overlapping pixels. It is important to consider the spatial resolution of the resampled compounded volume. While a fine resolution results in a large but highly sparse volume, a coarse resolution results in a small but dense volume. Note that because we use gradient information in the final alignment step, a too sparse volume precludes capturing inter-slice gradient information.

3.3 Initial alignment

In order to guess the initial alignment, we define a simple sweep procedure to limit the variability in the translational and angular positioning of the iUS probe during the acquisition. The procedure consists in a single axial sweep along the caudo-cranial direction, starting from the inferior extremity up to the superior extremity of the vertebra, with the probe orientation roughly normal to the coronal plane (Fig. 2a).

Similar to the approach proposed by Nagpal et al. [19], we consider that both CT and iUS images represent the same vertebra. In clinic, the vertebral level is identified before the surgical opening with palpation and confirmed by 2D fluoroscopy. Acquiring iUS images of the required vertebra is left to the surgeon's expertise. Although automatic methods to identify the vertebra extents on iUS images would be desired, this is beyond the scope of this paper. For now, we assume that the iUS scan is performed such that the same number of vertebrae appears in iUS and CT images. Thus, the center of mass of the iUS frame roughly corresponds to the center of the CT image. Note that although this center point, on both CT and iUS images, does not necessarily correspond to the anatomical center of the vertebra, the constrained probe orientation provides a roughly good estimate of the initial rotation. The proposed acquisition procedure constrains the scan trajectory to be approximately linear along the inferior to superior axis. Moreover, on the iUS image plane, the proximal to distal axis from the probe's transducers corresponds to the posterior to anterior axis on the vertebra. Based on these properties, the caudo-cranial direction of the iUS scan trajectory is estimated using a linear regression of the 3D coordinates of image centers. Then, three anatomical points can be created on the physical space (see Fig. 2b): a center of mass $\mathbf{p}_{\text{mass}}^{\text{US}}$, a superior point $\mathbf{p}_{\text{sup}}^{\text{US}}$ at a 10 mm distance from $\mathbf{p}_{\text{mass}}^{\text{US}}$ toward the superior direction, and a distal point $\mathbf{p}_{\text{distal}}^{\text{US}}$ at a 10 mm distance from $\mathbf{p}_{\text{mass}}^{\text{US}}$ toward the anterior direction. Similarly, three homologous points $\mathbf{p}_{\text{mass}}^{\text{CT}}$, $\mathbf{p}_{\text{sup}}^{\text{CT}}$ and $\mathbf{p}_{\text{distal}}^{\text{CT}}$ are created on the CT image, pre-operatively. Finally, the initial alignment transform \mathbf{T}^{init} is obtained by minimizing the least-square distances between the CT and the iUS points.

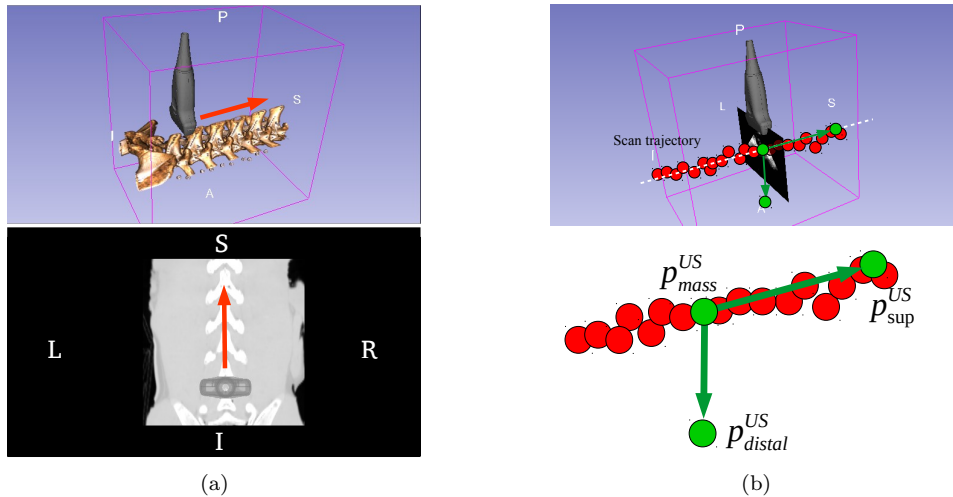


Fig. 2: Ultrasound acquisition procedure: (a) illustration of the iUS acquisition sweep direction, and (b) extraction of anatomy points from the iUS scan trajectory (red circles represent image centers)

3.4 Gradient alignment registration

The initial alignment approach roughly registers the CT to iUS images, based on the acquisition procedure described in Section 3.3. To refine the registration, we perform a gradient alignment registration [28]. The approach consists in using the orientation of the image intensity gradient vectors to estimate the similarity between two images. The similarity metric is given by the inner product between normalized gradients:

$$S(\nabla I_{US}(\mathbf{x}), \nabla I_{CT}(\mathbf{x})) = \left\langle \frac{\nabla I_{US}(\mathbf{x})}{|\nabla I_{US}(\mathbf{x})|}, \frac{\nabla I_{CT}(\mathbf{x})}{|\nabla I_{CT}(\mathbf{x})|} \right\rangle^n, \quad (1)$$

where \mathbf{x} is the image coordinate vector, ∇I_{US} and ∇I_{CT} correspond to the gradient of the fixed *iUS compounded volume* and the moving *CT volume of the extracted posterior surface*, respectively, and $n \in \mathbb{N}$ is a free parameter which characterizes the matching criterion and was set to $n = 64$ (as suggested in [29]). Gradient images ∇I_{US} and ∇I_{CT} are computed on GPU by convolving the image with a Gaussian derivative operator. Evaluation of the similarity metric in Eq. 1 is also performed on a GPU to accelerate the processing.

Covariance matrix adaptation evolution strategy (CMA-ES) [30] has been shown to provide good results for rigid vertebra registration [22,23], and was used to optimize for the final registration transform, given by:

$$T^{\text{reg}} = \arg \max_T S(\nabla I_{US}(\mathbf{x}), \nabla I_{CT}(T(\mathbf{x}))). \quad (2)$$

We modified the algorithm to take into account the vertebra surface on the intra-operative images. In the original approach, the metric is computed on a subset of points sampled from the image with high gradient magnitude, which has been shown to correspond to points with the lowest uncertainty [29]. In our approach, the points are sampled from a 2 mm thick region around the iUS extracted vertebra surface. Then, candidates satisfying the gradient magnitude criterion (i.e., with low uncertainty), were selected *among the vertebra surface points* to be used in Eq. 2. Our hypothesis is that gradient selectivity reduces the effect of surface extraction errors on the registration accuracy. The gradient orientation alignment metric implies that candidate gradients among the vertebra surface have a high gradient magnitude. Consequently, candidates with low gradient magnitude (high uncertainty) are discarded, which reduces risks of evaluating the metric on homogeneous regions that tend to be non-surface voxels.

Finally, we perform the registration using a multi-scale approach. Two different scales are used ($K = 2$). In the first pass, the images are smoothed using a Gaussian filter with $\sigma = 2$ mm to capture large structures, e.g., thicker surface of the vertebra. A second registration pass is performed on images filtered with $\sigma = 1$ mm.

Vertebra level	CT sub-volumes		Ultrasound (Axial centered)	
	size in voxels	size in mm	compounded volume (mm)	trajectory (mm)
T15	$512 \times 512 \times 17$	$180 \times 180 \times 34$	$85.5 \times 172.5 \times 133.5$	44.55
L1	$512 \times 512 \times 18$	$180 \times 180 \times 36$	$81 \times 163.5 \times 123$	38.24
L2	$512 \times 512 \times 20$	$180 \times 180 \times 40$	$112.5 \times 163.5 \times 123$	42.80
L3	$512 \times 512 \times 20$	$180 \times 180 \times 40$	$81 \times 163.5 \times 127.5$	41.66
L4	$512 \times 512 \times 20$	$180 \times 180 \times 40$	$91.5 \times 162 \times 120$	46.16
L5	$512 \times 512 \times 22$	$180 \times 180 \times 44$	$88.5 \times 160.5 \times 120$	44.94
L6	$512 \times 512 \times 18$	$180 \times 180 \times 36$	$84 \times 162 \times 127.5$	40.07

Table 1: CT sub-volumes and iUS acquisition details

4 Evaluation

4.1 Data

In this study, we used the same data described in [16]. The dataset consists in lumbosacral section of a porcine cadaver that underwent a CT and iUS scans. A PQ6000 CT scanner (Picker International Inc., Cleveland, OH, United States) was used to acquire images of vertebrae T15 to L6. The scan was performed from anatomical superior to inferior direction with the specimen placed in supine position. The CT images have a resolution of $0.35 \times 0.35 \text{ mm}^2$ and a slice thickness of 2 mm. The entire CT volume was divided into sub-volumes, each one containing a single vertebra (Table 1). Using fiducial markers, a ground truth registration transform was obtained for each vertebra (see [16] for details).

4.2 Measurements

Because the fiducials were placed far from the vertebra surface, a small misalignment of the fiducial points may result in a large TRE at the vertebra surface. Therefore, the fiducial registration error (FRE), computed on fiducial locations, may not be representative of the registration accuracy. To evaluate the quality of the registration, TRE was computed on seven landmarks manually identified on the surface of each vertebra on the CT images. The anatomical landmarks correspond to: a point on the apex of the spinous process, two points on the left and right laminae, two points on the left and right superior articular processes and two points on the left and right inferior articular processes. The TRE of each vertebra is obtained by:

$$TRE_v = \sqrt{\frac{1}{7} \sum_{i=1}^7 |T^{\text{gt}} \mathbf{p}_i - T^{\text{reg}} \mathbf{p}_i|^2}, \quad (3)$$

where v is the vertebral level, T^{gt} is the ground truth registration transform obtained from fiducial point-based registration, T^{reg} is the computed registration transform and \mathbf{p}_i is the i^{th} landmark point manually positioned on the vertebra surface. As determined by the consensus report on spine IGS [31], we fix the acceptance threshold for successful registrations to 2 mm. We report the success rate (in %) as the fraction of registration trials achieving a TRE below 2 mm.

In addition to registration accuracy, we measured the computation time required to perform the registration of each vertebra. The computations involve three main tasks: extracting the vertebra surface (backward tracing), compounding the iUS volume and aligning CT to iUS volumes (i.e., solving Eq. 2). We also report the computation time required to perform the initial alignment, although it can be neglected due to its small contribution to the overall registration time. Note that the iUS acquisition time, i.e., the time required to manipulate the iUS probe and perform the sweep, is not reported in this study, but takes approximately 20 s. All computations were performed using an Intel[®] Core[™] i7-3820 CPU at 3.6 GHz \times 8 station and a NVIDIA GeForce GTX 670 graphics card with 4 Gb of memory.

4.3 Experiments

Two experiments were carried out with the following goals: 1) to assess the overall registration accuracy and the effect of the iUS acquisition sweep on the registration and 2) to assess the effect of the iUS volume compounding and acquisition frame rate on the registration accuracy and computation time.

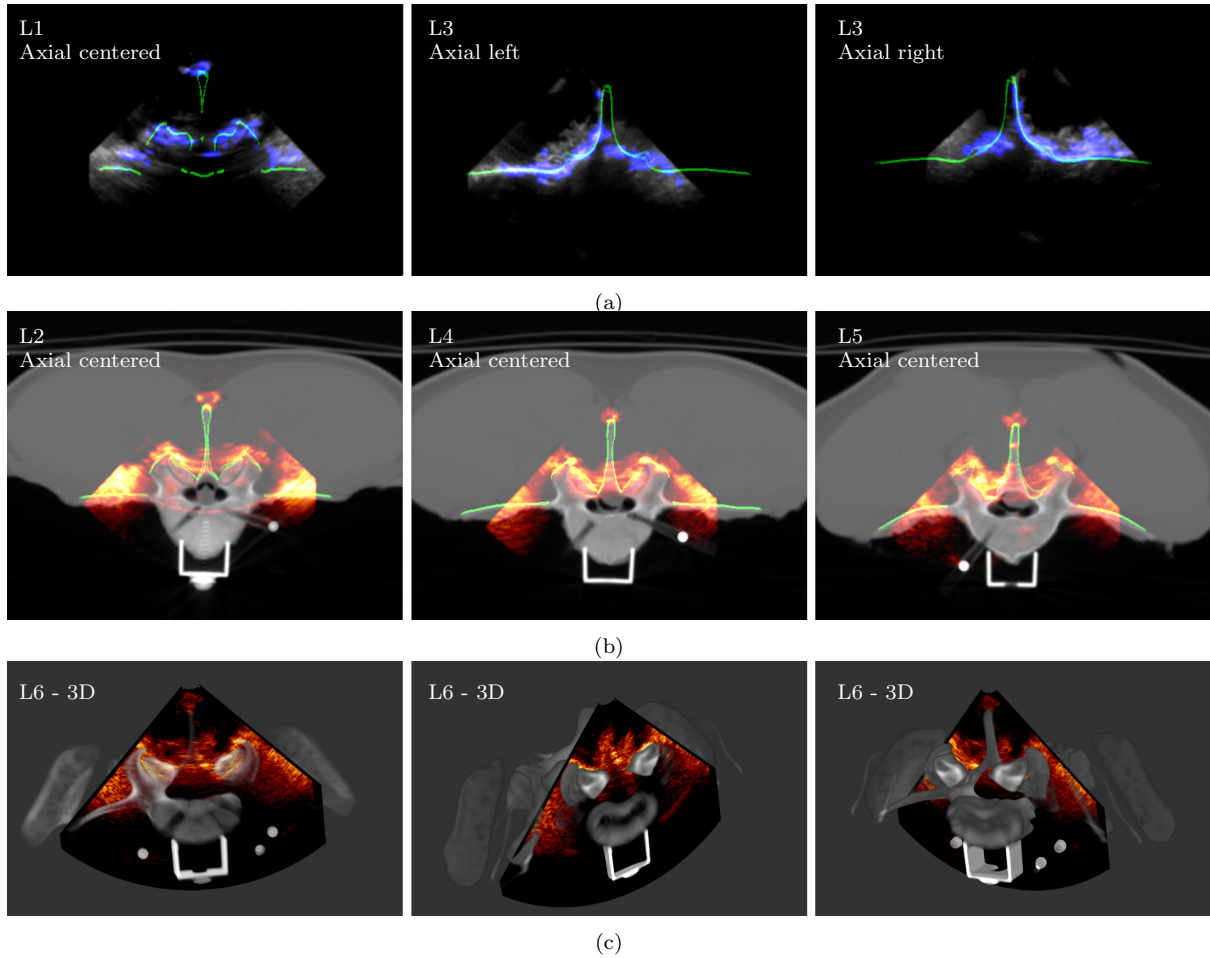


Fig. 3: Qualitative registration results at various vertebral levels: a) alignment of iUS image (gray), iUS extracted posterior surface of vertebra (blue) and CT extracted posterior surface of vertebra (green); b) alignment of iUS image (heat map), CT image (gray) and CT extracted posterior surface of vertebra (green); c) 3D views of iUS slice aligned with CT volume.

4.3.1 Experiment 1: sensitivity to iUS acquisition

We use three iUS acquisitions that satisfy the requirements of the procedure described in Section 3.1. Each acquisition consists in a single axial sweep at approximately 3 cm posterior to the apex of the spinous process, such that: A1 is centered on the spinous process (ultrasound sweep No. 1 in [16]), A2 is 1 cm to the left of the spinous process (ultrasound sweep No. 2 in [16]), and A3 is 1 cm to the right of the spinous process (ultrasound sweep No. 3 in [16]). Note that for consistency the sweep directions were inverted to match the inferior to posterior direction.

For each vertebra, 100 registration trials were performed to account for the stochastic nature of the CMA-ES optimizer. The vertebra surface extraction on the iUS images and the volume compounding were performed every 10 trials to measure the computation time. We set $d = 0.5$ mm for acquisition sub-sampling (see Section 3.1). The resolution of the iUS compounded volume is set to $1.5 \times 1.5 \times 1.5$ mm³, to produce sufficiently dense volumes. In total, 100 registrations \times 7 vertebral levels \times 3 iUS acquisitions = 2,100 trials were performed.

4.3.2 Experiment 2: sensitivity to parameter variation

To evaluate the sensitivity of our registration approach to the iUS compounded volume resolution parameter R and the sub-sampling parameter d , we experimented the effect of different values on the registration

outcomes. Using the axial centered iUS acquisition A1, we varied the parameter R to take values in $\{0.5 \times 0.5 \times 0.5 \text{ mm}^3, 1 \times 1 \times 1 \text{ mm}^3, 1.5 \times 1.5 \times 1.5 \text{ mm}^3\}$ and the parameter d to take values in $\{0 \text{ mm}, 0.5 \text{ mm}, 1 \text{ mm}\}$. Similar to experiment 1, 100 registrations were performed for each vertebra. The vertebra surface extraction on the iUS images and the volume compounding were performed every 20 trials to measure the computation time. In total, 100 registrations \times 7 vertebral levels \times 3 sub-sampling rates \times 3 iUS volume compounding resolutions = 6,300 trials were performed in this experiment. Note that the reported results obtained with the downsampling parameter $d = 0.5 \text{ mm}$ and the iUS compounded volume resolution $R = 1.5 \times 1.5 \times 1.5 \text{ mm}^3$ have already been evaluated in experiment 1.

5 Results and discussion

Fig. 3 shows qualitative registration results obtained for different vertebrae with the proposed framework. The iUS images appear to be aligned with the surface of the vertebra on the CT image. The registration can be visually assessed based on the apex of the spinous process and the inferior articular processes.

5.1 Results of experiment 1

Accuracy and computation time results for the three iUS acquisitions are summarized in Table 2. The overall TRE for each acquisition is slightly better than the results reported in [16]. The axial centered acquisition A1 yielded the best results with a median TRE of 1.48 mm (IQR 0.68 mm) which is below the acceptance threshold of 2 mm with a success rate of 84.42%.

Notice that the results obtained at L4 seem to be the worst, with a median TRE of 2.03 mm, 2.07 mm and 2.36 mm with A1, A2 and A3, respectively. We suspect the reason behind this large error to be related to the large FRE of 0.593 mm induced when the ground truth registration was generated at L4. In fact, since the fiducials were intentionally placed far from the vertebra, in order to preclude interference with the iUS scans, a small value of the FRE would lead to a large displacement at the vertebra surface where the TRE is being computed. Therefore, the assessment of the accuracy at L4 is rendered less reliable. Considering the established 2 mm-increments breach grading system (intrapedicular, 0–2 mm breach, 2–4 mm breach, > 4 mm breach) [32,33], we define the threshold value of 4 mm to represent a *major registration failure*. The error range reported at L4 is between 1.25 mm and 3.14 mm, preventing major failures. Over the 2,100 trials, we note 7 cases (< 0.004%) of major failures.

The number of selected frames and the computation time for each vertebra registration of the axial centered acquisition A1 are detailed in Table 3. The average overall registration time is $0.742 \text{ s} \pm 0.037 \text{ s}$ per vertebra. This includes both the initial alignment and the gradient alignment processing times. Including the reconstruction and the registration, the total procedure time is $10.79 \text{ s} \pm 1.27 \text{ s}$, which is practical in the OR. In fact, this is significantly lower than the 2 min reported by Yan et al. [17] and the 100 s reported by Koo et al. [18] per each vertebra registration. The registration time ranging between 50–185 s reported by Nagpal et al. [19] involved multiple vertebrae registration, precluding a direct comparison. It should be noted that all the aforementioned works did not include the iUS volume reconstruction time, which is expected to be performed after acquiring the iUS images during the surgery. In our approach, the computational bottleneck is associated with the reconstruction step with a 93% contribution to the overall registration time. Further improvements to reduce the computation time for the posterior surface of vertebra extraction and the iUS volume compounding could be the subject of future work.

During the iUS acquisition, two types of variations can occur: 1) small variations of the probe positions (noise) along every direction caused by inadvertent hand motions, and 2) accumulation of variations that cause a drift of the acquisition trajectory. Our method aims at finding the linear trajectory of the probe. Therefore, compared to the average length of the probe’s trajectory of 4.2 cm (see Table 1), the residual noise is assumed to be significantly smaller and normally distributed along each direction. On the other hand, acquisition drifts are more likely to occur along the posterior-anterior axis than in the left-right axis, due to the superior-anterior cavity opening. As an effect, the linear regression would yield a rotational misalignment around the left-right axis. In our experiment, the iUS scans were acquired in a realistic scenario, i.e., in a standard open-back spine surgery on a porcine cadaver. The left-right as well as posterior-anterior variations are taken into consideration, as the acquisitions were manually performed. The results obtained demonstrate that our registration approach allows to recover from the variations in the 21 evaluated acquisitions.

Table 2: Registration accuracy and computation time results for each iUS acquisition.

	Vertebra level	Initial alignment TRE (mm)	Final TRE (mm)			Success rate (%)	Time (s)
			Median	IQR	Range		
Axial centered	T15	3.71	1.20	0.30	[0.60, 1.88]	100	13.72
	L1	2.92	0.84	0.32	[0.45, 1.39]	100	10.56
	L2	2.44	1.37	0.44	[0.61, 2.21]	95	11.12
	L3	3.70	1.40	0.32	[0.83, 2.21]	98	10.06
	L4	5.92	2.03	0.35	[1.36, 2.78]	47	10.26
	L5	8.32	1.69	0.42	[0.95, 2.47]	79	10.38
	L6	9.18	1.75	0.46	[1.09, 2.66]	72	9.48
All vertebrae			1.48	0.68		84.42	10.79
Yan et al. [16]			1.93	0.72			
Axial left	T15	7.37	1.60	0.66	[0.80, 14.16]	80	12.95
	L1	8.23	1.72	0.73	[0.72, 2.95]	72	14.08
	L2	7.07	1.63	0.58	[0.60, 2.87]	81	9.79
	L3	9.93	1.89	0.90	[0.87, 2.95]	54	12.33
	L4	10.87	2.07	0.40	[1.25, 2.89]	42	11.21
	L5	10.65	1.67	0.49	[1.04, 2.55]	82	11.97
	L6	10.88	1.54	0.33	[0.82, 21.04]	89	9.05
All vertebrae			1.69	0.63		71.42	11.63
Yan et al. [16]			2.31	1.17			
Axial right	T15	4.95	1.20	0.52	[0.40, 2.18]	97	10.22
	L1	6.64	0.84	0.31	[0.34, 1.52]	100	9.83
	L2	7.30	1.62	0.33	[0.83, 2.21]	92	11.69
	L3	7.20	1.85	0.44	[1.10, 2.79]	65	11.72
	L4	11.61	2.36	0.38	[1.70, 3.14]	6	10.30
	L5	11.59	1.82	0.57	[1.05, 12.83]	64	11.57
	L6	9.54	1.94	0.46	[1.06, 3.53]	55	8.75
All vertebrae			1.70	0.78		68.42	10.58
Yan et al. [16]			1.93	1.38			

TRE: target registration error, IQR: interquartile range.

Table 3: Computation time results for the axial centered acquisition.

Vertebra level	Frames		Computation time (s)				Total
			Reconstruction		Registration		
	Total	Selected	Surface extraction	Volume compounding	Initial alignment	Gradient alignment	
T15	197	106 (53%)	8.00	4.93	0.044	0.736	13.72
L1	209	80 (38%)	6.04	3.81	0.045	0.667	10.56
L2	219	83 (37%)	6.26	4.12	0.045	0.695	11.12
L3	215	76 (35%)	5.75	3.58	0.044	0.680	10.06
L4	205	79 (38%)	5.92	3.59	0.045	0.707	10.26
L5	211	81 (38%)	6.09	3.54	0.046	0.702	10.38
L6	235	76 (32%)	5.70	3.04	0.046	0.693	9.48
Average	–	–	6.25	3.80	0.045	0.69	10.79

The stochastic outcome of the CMA-ES optimization method yields a variability in the TRE results. However, the interquartile ranges of 0.68 mm, 0.63 mm and 0.78 mm obtained using the centered axial, the left axial and the right axial acquisitions, respectively, are smaller than those reported in [16] with different initial starts. In a clinical context, the robustness of the method is critical for the registration to be practical in IGS. While major registration failures (TRE > 4 mm) are visually identifiable during surgery, allowing appropriate decisions to be taken (e.g., re-scanning the vertebra or re-running the registration), registration failures resulting in a TRE ranging between 2 mm and 4 mm are harder to be detected visually. Our registration approach showed a good statistical robustness to CMA-ES variability with an average success rate of 84.42% over the 700 trials when using the centered axial acquisition.

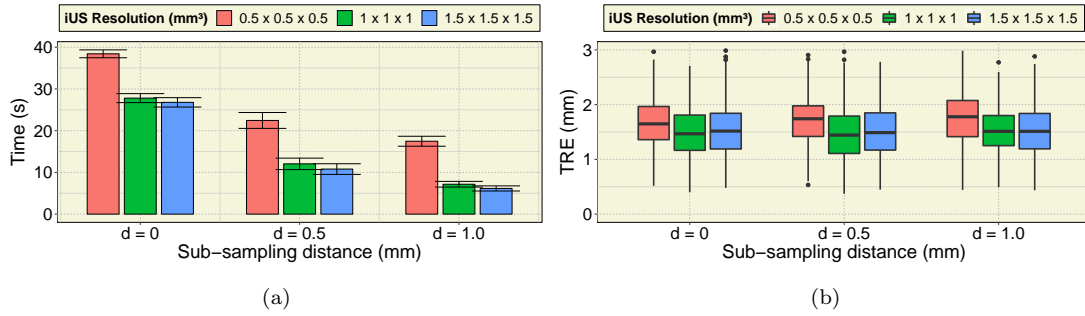


Fig. 4: Results of experiment 2 on the sensitivity to the sub-sampling (frame rate) parameter d and the iUS volume resolution parameter R : (a) computation time results, and (b) accuracy results.

5.2 Results of experiment 2

Fig. 4 shows the effect of the frame rate sub-sampling and the compounded volume resolution on the registration accuracy and computation time. A repeated measure analysis of variance (ANOVA) test showed that reducing the number of acquisition frames allows to reduce the reconstruction time without a significant effect on the accuracy ($F_{2,12} = 1.10, p = 0.36$). On the other hand, although the computation time decreases with a coarser resolution, the registration accuracy is affected ($F_{2,12} = 12.01, p = 0.001$).

In a clinical context, the trade-off between speed and accuracy is important. While the overall accuracy showed good robustness to coarse resolutions (overall median TRE of 1.56 mm and IQR = 0.67 mm), the registration time varied significantly from 40.25 s for fine resolutions to 5.61 s for coarse resolutions. A compromise between speed and accuracy suggests a sub-sampling rate of $d = 0.5$ mm and an iUS compounding volume resolution between $R = 1 \times 1 \times 1$ mm³ and $R = 1.5 \times 1.5 \times 1.5$ mm³.

6 Conclusion

Rapid and accurate CT-to-iUS registration of the vertebrae is crucial for spine surgical navigation procedures. During the intervention, patient movement, bone removal and drilling instrumentations or contact with the tracked reference may invalidate the registration. In this case, the registration procedure has to be recomputed efficiently. This paper presents a framework to rigidly align pre-operative CT with the intra-operative ultrasound images of a single vertebra. Experiments conducted with multiple iUS acquisitions on a lumbosacral section of a porcine cadaver yielded an overall median accuracy of 1.48 mm with ~ 11 s of computation time when using the proposed iUS sweeping procedure. The method is robust, as shown with off center iUS sweep accuracies of 1.69 mm and 1.70 mm. With a clinically acceptable accuracy below 2 mm and a straightforward iUS acquisition procedure, the approach can be easily integrated into the surgical workflow. The entire registration procedure is expected to be completed in less than a minute, which includes preparing the cavity with a saline solution, acquiring iUS images and performing the registration. This would significantly reduce the typical 15-30 minutes required for intra-operative CT imaging (time includes: draping the patient, adjusting patient table, positioning the scanner, requiring the staff to leave the OR for radiation safety, acquiring the images and removing the scanner), without additional exposure to radiation.

Rigid registration is adapted to the bony structure of the vertebra. However, because of the spine curvature flexibility, this statement becomes less valid as the number of vertebrae in a single scan increases. Abdominal respiratory motions or changes between the pre-operative supine posture and intra-operative prone posture of the patient may induce deformations of the spinal column. Therefore, it is important to account for the spine curvature, especially in the cervical section, where the intervertebral displacement can be large. Moreover, anatomical structure of the spine differs in the cervical, thoracic and lumbar sections, thus, the accuracy required in fusion surgery varies accordingly. Our future work will focus on investigating effects of the anatomy on rigid registration in the thoracic and cervical sections.

Compliance with ethical standards

Funding This study was funded by grants from the Canadian Institutes of Health Research (246067) and from the Natural Sciences and Engineering Research Council of Canada (396395).

Conflict of interest None.

Ethical approval This article does not contain any studies with animal or human participants performed by any of the authors.

Informed consent This article does not contain patient data.

References

1. Rajaei, S.S., Delamarter, R.B.: Spinal Fusion in the United States. *Spine* **37**(1), 67–76 (2012)
2. Bernstein, D.N., Brodell, D., Li, Y., Rubery, P.T., Mesfin, A.: Impact of the Economic Downturn on Elective Lumbar Spine Surgery in the United States : A National Trend Analysis , 2003 to 2013. *Global Spine Journal* **7**(3), 213–219 (2017)
3. Mac-Thiong, J.M., Parent, S., Poitras, B., Joncas, J., Hubert, L.: Neurological outcome and management of pedicle screws misplaced totally within the spinal canal. *Spine* **38**(3), 229–237 (2013)
4. Su, A.W., Habermann, E.B., Thomsen, K.M., Milbrandt, T.A., Nassr, A., Larson, A.N.: Risk Factors for 30-Day Unplanned Readmission and Major Perioperative Complications After Spine Fusion Surgery in Adults: A Review of the National Surgical Quality Improvement Program Database. *Spine* **41**(19), 1523–1534 (2016)
5. Rahmathulla, G., Nottmeier, E.W., Pirris, S.M., Deen, H.G., Pichelmann, M.A.: Intraoperative image-guided spinal navigation: technical pitfalls and their avoidance. *Neurosurgical Focus* **36**(3), E3 (2014)
6. Smith, Z.A., Sugimoto, K., Lawton, C.D., Fessler, R.G.: Incidence of Lumbar Spine Pedicle Breach After Percutaneous Screw Fixation A Radiographic Evaluation of 601 Screws in 151 Patients. *Journal of Spinal Disorders and Techniques* **27**(7), 358–363 (2014)
7. Austin, M.S., Vaccaro, A.R., Brislin, B., Nachwalter, R., Hilibrand, A.S., Albert, T.J.: Image-Guided Spine Surgery A Cadaver Study Comparing Conventional Open Laminoforaminotomy and Two Image-Guided Techniques for Pedicle Screw Placement in Posterolateral Fusion and Nonfusion Models. *Spine* **27**(22), 2503–2508 (2002)
8. Gebhard, F., Weidner, A., Liener, U.C., Stckle, U., Arand, M.: Navigation at the spine. *Injury* **35**(1, Supplement), 35 – 45 (2004)
9. Yan, C.X., Goulet, B., Pelletier, J., Chen, S.J.S., Tampieri, D., Collins, D.L.: Towards accurate, robust and practical ultrasound-CT registration of vertebrae for image-guided spine surgery. *International Journal of Computer Assisted Radiology and Surgery* **6**(4), 523–537 (2011)
10. Arand, M., Hartwig, E., Kinzl, L., Gebhard, F.: Spinal navigation in tumor surgery of the thoracic spine: first clinical results. *Clinical Orthopaedics and Related Research* **399**, 211–218 (2002)
11. Costa, F., Dorelli, G., Ortolina, A., Cardia, A., Attuati, L., Tomei, M., Milani, D., Balzarini, L., Galbusera, F., Morengi, E., Fornari, M.: Computed Tomography-Based Image-Guided System in Spinal Surgery State of the Art Through 10 Years of Experience. *Operative Neurosurgery* **11**(1), 59–68 (2015)
12. Tabaraee, E., Gibson, A.G., Karahalios, D.G., Potts, E.A., Mobasser, J.P., Burch, S.: Intraoperative cone beam-computed tomography with navigation (O-ARM) versus conventional fluoroscopy (C-ARM): A cadaveric study comparing accuracy, efficiency, and safety for spinal instrumentation. *Spine* **38**(22), 1953–1958 (2013)
13. Rampersaud, Y.R., Foley, K.T., Shen, A.C., Williams, S., Solomito, M.: Radiation Exposure to the Spine Surgeon During Fluoroscopically Assisted Pedicle Screw Insertion. *Spine* **25**(20), 2637–2645 (2000)
14. Scheufler, K.M., Franke, J., Eckardt, A., Dohmen, H.: Accuracy of image-guided pedicle screw placement using intraoperative computed tomography-based navigation with automated referencing, part I: Cervicothoracic spine. *Neurosurgery* **69**(4), 782–795 (2011)
15. Quiñones-Hinojosa, A., Kolen, E.R., Jun, P., Rosenberg, W.S., Weinstein, P.R.: Accuracy over space and time of computer-assisted fluoroscopic navigation in the lumbar spine in vivo. *Clinical Spine Surgery* **19**(2), 109–113 (2006)
16. Yan, C.X.B., Goulet, B., Chen, S.J.S., Tampieri, D., Collins, D.L.: Validation of automated ultrasound-CT registration of vertebrae. *International Journal of Computer Assisted Radiology and Surgery* **7**(4), 601–610 (2012)
17. Yan, C.X., Goulet, B., Tampieri, D., Collins, D.L.: Ultrasound-CT registration of vertebrae without reconstruction. *International Journal of Computer Assisted Radiology and Surgery* **7**(6), 901–909 (2012)
18. Koo, T.K., Kwok, W.E.: Hierarchical CT to Ultrasound Registration of the Lumbar Spine: A Comparison with Other Registration Methods. *Annals of Biomedical Engineering* **44**(10), 2887–2900 (2016)
19. Nagpal, S., Abolmaesumi, P., Rasoulia, A., Hacihaliloglu, I., Ungi, T., Osborn, J., Lessoway, V.A., Rudan, J., Jaeger, M., Rohling, R.N., Borschneck, D.P., Mousavi, P.: A multi-vertebrae CT to US registration of the lumbar spine in clinical data. *International Journal of Computer Assisted Radiology and Surgery* **10**(9), 1371–1381 (2015)
20. Gueziri, H.E., Collins, D.L.: Fast Registration of CT with Intra-operative Ultrasound Images for Spine Surgery. In: *Computational Methods and Clinical Applications for Spine Imaging*, pp. 29–40. Springer International Publishing (2019)
21. Brendel, B., Rick, S.W.A., Stockheim, M., Ermert, H.: Registration of 3D CT and Ultrasound Datasets of the Spine using Bone Structures. *Computer Aided Surgery* **7**(3), 146–155 (2002)
22. Winter, S., Brendel, B., Pechlivanis, I., Schmieder, K., Igel, C.: Registration of CT and Intraoperative 3-D Ultrasound Images of the Spine Using Evolutionary and Gradient-Based Methods. *IEEE Transactions on Evolutionary Computation* **12**(3), 284–296 (2008)

23. Gill, S., Abolmaesumi, P., Fichtinger, G., Boisvert, J., Pichora, D., Borshneck, D., Mousavi, P.: Biomechanically constrained groupwise ultrasound to CT registration of the lumbar spine. *Medical Image Analysis* **16**(3), 662–674 (2012)
24. Rasoulian, A., Abolmaesumi, P., Mousavi, P.: Feature-based multibody rigid registration of CT and ultrasound images of lumbar spine. *Medical Physics* **39**(6), 3154–3166 (2012)
25. Moghari, M.H., Abolmaesumi, P.: Point-Based Rigid-Body Registration Using an Unscented Kalman Filter. *IEEE Transactions on Medical Imaging* **26**(12), 1708–1728 (2007)
26. Hacıhaliloglu, I.: Enhancement of bone shadow region using local phase-based ultrasound transmission maps. *International Journal of Computer Assisted Radiology and Surgery* **12**(6), 951–960 (2017)
27. Drouin, S., Kochanowska, A., Kersten-Oertel, M., Gerard, I.J., Zelmann, R., De Nigris, D., Bériault, S., Arbel, T., Sirhan, D., Sadikot, A.F., Hall, J.A., Sinclair, D.S., Petrecca, K., DelMaestro, R.F., Collins, D.L.: IBIS: an OR ready open-source platform for image-guided neurosurgery. *International Journal of Computer Assisted Radiology and Surgery* **12**(3), 363–378 (2017)
28. De Nigris, D., Collins, D.L., Arbel, T.: Fast rigid registration of pre-operative magnetic resonance images to intra-operative ultrasound for neurosurgery based on high confidence gradient orientations. *International Journal of Computer Assisted Radiology and Surgery* **8**(4), 649–661 (2013)
29. De Nigris, D., Collins, D.L., Arbel, T.: Multi-modal image registration based on gradient orientations of minimal uncertainty. *IEEE Transactions on Medical Imaging* **31**(12), 2343–2354 (2012)
30. Hansen, N., Ostermeier, A.: Completely derandomized self-adaptation in evolution strategies. *Evolutionary computation* **9**(2), 159–195 (2001)
31. Cleary, K., Anderson, J., Brazaitis, M., Devey, G., DiGioia, A., Freedman, M., Grönemeyer, D., Lathan, C., Lemke, H., Long, D., Mun, S.K., Taylor, R.: Final report of the technical requirements for image-guided spine procedures workshop. *Computer Aided Surgery* **5**(3), 180–215 (2000)
32. Kuklo, T.R., Lenke, L.G., Obrien, M.F., Lehman Jr, R.A., Polly Jr, D.W., Schroeder, T.M.: Accuracy and efficacy of thoracic pedicle screws in curves more than 90. *Spine* **30**(2), 222–226 (2005)
33. Guha, D., Jakubovic, R., Gupta, S., Alotaibi, N.M., Cadotte, D., da Costa, L.B., George, R., Heyn, C., Howard, P., Kapadia, A., Klostranec, J.M., Phan, N., Tan, G., Mainprize, T.G., Yee, A., Yang, V.X.: Spinal intraoperative three-dimensional navigation: correlation between clinical and absolute engineering accuracy. *Spine Journal* **17**(4), 489–498 (2017)